Virtual gravitational wave interferometers with actual mirrors

Alain Brillet* and Jean-Yves Vinet†
C.N.R.S., Observatoire de la Côte d'Azur, Nice 06304, France

Vincent Loriette‡
C.N.R.S., Laboratoire d'Optique Physique UPR A0005, Ecole Supérieure de Physique et Chimie Industrielles, 10, rue Vauquelin, 75005 Paris, France

Jean-Marie Mackowski,§ Laurent Pinard,‖ and Alban Remillieux¶
C.N.R.S., Service des Matériaux Avancés, Bât. 213, Institut de Physique Nucléaire de Lyon, 22, Boulevard Niels Bohr, 69622 Villeurbanne, France

(Received 3 February 2003; published 27 May 2003)

Long base interferometers for gravitational wave detection involve a number of mirrors having outstanding levels of quality. These large mirrors are now currently being produced. Each mirror has its own signature in reflected wave fronts due to its particular roughness pattern. Direct wave front measurements, carried out after the coating process, provide numerical maps from which very useful information can be extracted, either directly or by insertion in a numerical model of the interferometer. In particular, we show how it is possible to test the performances of the instrument for various attitudes of the mirrors before installing them in the vacuum chambers, a heavy and dangerous task.

DOI: 10.1103/PhysRevD.67.102006 PACS number(s): 04.80.Nn, 06.20.−f, 07.05.Tp, 07.60.Ly

I. INTRODUCTION

The detection bandwidth of large interferometric gravitational wave detectors, such as Virgo and the Laser Interferometric Gravitational Wave Observatory (LIGO) [1,2], will extend from a few Hz to a few kHz. In most of that range, from about 100 Hz up to the upper limit, their performance will be limited by the quality of the large optical components.

It is important to recall briefly what is their common optical design: these are Michelson interferometers operated as close as possible to the dark fringe. Each (3 or 4 km) arm of the Michelson interferometer is a Fabry-Perót resonant cavity, which provides an effective length of more than 100 km. The laser light which remains in the ''bright fringe'' reflected by the Michelson interferometer is ''recycled'' towards the beam splitter in order to enhance the effective laser power, and hence to improve the shot noise–limited measurement noise. Nominally, the optical beam geometry is simple: the laser beam is a TEM_{00} Gaussian mode which matches the eigenmodes of the arms resonant cavities.

The properties of the mirror surfaces and coatings are important for two reasons:

Individual mirror losses determine how much light is lost by transmission, absorption, and scattering at large angles. Neglecting the fact that scattered light can create additional noise [4,5] if it finds a path to recombine with the main beam, we can consider these as a simple loss which decreases the efficiency of the recycling process.

Low angle scattering plays a different role when the light is scattered out of the TEM_{00} mode but couples to low order modes and remains inside the resonant cavities. The effect is not only to decrease the recycling coefficient (and thus the signal amplitude), but also to add spurious light on the dark fringe, and then to increase the shot noise.

An important issue is finally the level of asymmetry of the two arms of the Michelson interferometer. For a given average level of mirror imperfection, the overall performance of the interferometer will improve if the symmetry is improved. We have shown earlier [6] that specific and powerful optical modeling tools were necessary in order to specify the performances of the mirrors. In this paper we show that the same tools are useful again once the mirrors have been realized and measured: using the measured mirrors maps, we build a complete numerical interferometer, which allows us to ''manipulate'' them safely and quickly, in order to optimize their choice and relative positioning.

We also use this technique to optimize the performance of the mode cleaner: in Virgo, this is [3] a high finesse ring cavity of triangular shape; two flat mirrors operate with an incidence angle of about 45°, while the third, curved mirror operates with a very small incidence angle of about 300 μRd. It is important to decouple very well the two possible beams (clockwise and counter clockwise), so we have to minimize the backscatter from one beam to the other, and since the residual roughness of the mirror is not axisymmetric, the performance will depend on the rotation angle of the mirror around its axis, and can be optimized through the simulation. In both cases, we show how to handle these maps and avoid slow and difficult experimental studies.

*Electronic address: brillet@obs-nice.fr
†Electronic address: vinet@obs-nice.fr
‡Electronic address: loriette@optique.espci.fr
§Electronic address: Mackowski@ipnl.in2p3.fr
‖Electronic address: Pinard@ipnl.in2p3.fr
¶Electronic address: alban.remillieux@ipnl.in2p3.fr

II. METROLOGY AND WAVE FRONT MEASUREMENTS

The mirror surface figures are obtained using a phase shifting Fizeau interferometer. In order to reach a measurement accuracy better than 10 nm, required for testing Virgo optics, the instrument was designed to be as aberration-free as possible. In particular it does not contain any zoom optics, thus its resolution is fixed. Each pixel of the charge-coupled device (CCD) array images a 350 μm$\times$350 μm surface. The required accuracy is by far better than any commercially available large diameter reference flat. All reference flats are tested against each other using the standard *three flats test* technique which provides absolute surface figure measurements on a number of diameters of each reference flat [8]. Some mirrors are larger than the Fizeau 150 mm aperture; we have developed a stitching algorithm which allows us to perform subaperture measurements and successfully combine them into a full map. The loss of accuracy introduced by the stitching technique lies in the nanometer range, so it does not degrade significantly the overall performances of the instrument. The instrument provides discrete surface figure maps, corrected from the reference flats surface figures, on 430×430 grids for single aperture maps, and up to 1000×1000 grids for large maps that require the stitching technique. Because the Fizeau interferometer measures the air gap between the reference flat and the surface under study, the surface figure maps usually contain an arbitrary piston term as well as arbitrary tip or tilt terms.

III. NUMERICAL METHODS

A. Extraction of mirror parameters

The wave front maps coming from direct measurement need to be refined before exploitation. The reason is that in the numerical codes described above, we need to match the beams. For matching, it is necessary to have collimated mirrors of known curvature radius. It is therefore necessary to extract the tilt angles and the curvature radius from the empirical data. Tilt angles come from the fact that some wedge may exist in the substrate, and the curvature radius given by the manufacturer is usually within the requirements, but its value is not accurately known and, moreover it does not have the same meaning for the polisher and for the laser scientist. This last point notes a severe problem when defining the specifications of optical components. Usually, polishers define the radius of curvature as the radius of the sphere matching the surface figure over a fixed diameter. In this case all points on the surface are of equal importance for evaluating its value. On the other hand, since the mirrors are used with laser beams, it is clear that the value of the radius of curvature is more critical for regions close to the mirror center than for regions close to the mirror edge. The radius of curvature, as measured by polishers, which are dependent on a particular surface diameter, can only be used as an estimate of the quality of the polishing process, not as accurate information on the surface figure. It must therefore be understood that these three geometrical parameters (tilt angles, curvature radius), are not independent on the analyzing beam. If the analyzing beam is a clean Gaussian beam of width parameter w, the geometrical parameters are w dependent. But in turn, w, due to matching, depends on the curvature parameter, for we obviously want to take an analyzing value of w corresponding to a realistic operation of a defined cavity. As customary in such problems, an iterative approach allows us to reach the goal. We first choose an approximate value R_1 of the curvature radius (e.g. its nominal value), from which an estimate w_1 of w can be derived, knowing the geometry of the cavity in which the mirror is to be included and the wavelength of the light. We denote $\varphi_0(x,y)$ the fundamental TEM_{00} mode of width w_1, and arbitrary phase curvature radius R. We have, namely (in all of what follows, $k\equiv 2\pi/\lambda$),

$$\varphi_0(x,y)=\sqrt{\frac{2}{\pi w_1^2}}\exp[-(x^2+y^2)/w_1^2]\times\exp[ik(x^2+y^2)/2R].$$

If $z=f(x,y)$ is the apex equation of the mirror's surface, the reflected field is

$$\varphi_{\mathrm{ref}}(x,y)=\varphi_0(x,y)\times\exp[-2ikf(x,y)].$$

Now we shall consider a field $\varphi_{\mathrm{probe}}(x,y)$ coming from the mirror, with an arbitrary direction defined by the angles $(2\theta,\phi)$, as if it were reflected off a mirror tilted by (θ,ϕ), and the same arbitrary phase curvature radius R as the incoming field. We have, namely,

$$\varphi_{\mathrm{probe}}(x,y)=\sqrt{\frac{2}{\pi w_1^2}}\exp[-(x^2+y^2)/w_1^2]\times\exp[-ik(x^2+y^2)/2R]\times\exp[2ik\theta(x\cos\phi+y\sin\phi)].$$

We propose to find R,θ,ϕ by looking for the best coupling between φ_{ref} and φ_{probe}. In other words, we use the probe to test the preferred direction of the reflected field, and its preferred matching parameter. In this way we deduce the geometrical parameters of the mirror from the behavior of the probe. The coupling coefficient $\Gamma(R,\theta,\phi)$ is defined by the Hermitian scalar product

$$\Gamma(R,\theta,\phi)=\int_{\mathrm{R}^2}\overline{\varphi_{\mathrm{probe}}(x,y)\,\varphi_{\mathrm{ref}}(x,y)}\,dx\,dy.$$

This is

$$\Gamma(R,\theta,\phi)=\int_{\mathrm{R}^2}I_{w_1}(x,y)\exp\left[2ik\left(f(x,y)-\frac{x^2+y^2}{2R}-\theta(x\cos\phi+y\sin\phi)-p\right)\right]dx\,dy. \quad (1)$$

$I_{w_1}(x,y)$ is the normalized optical intensity distribution. p is a piston (corresponding to a possible longitudinal translation of the mirror surface). It is clear, however, that p does not contribute the modulus of Γ. The best coupling is obtained

TABLE I. Empirical statistical parameters of two mirrors recently manufactured for Virgo.

Mirror no.	Curvature radins	Matched waist	rms roughness
C01077	3584 m	2.12 cm	2.8 nm
C02017	3624 m	2.15 cm	3.6 nm

when $|\Gamma|^2$ is a maximum, so that the problem is reduced to maximizing $|\Gamma|^2$ with respect to R, θ, ϕ. Now, if the mirror is of high quality, the departure of the surface from an ideal paraboloid is very small, and when the probe parameters are near their optimal values, the residual

$$\delta f(x,y) = f(x,y) - \frac{x^2+y^2}{2R} - \theta(x\cos\phi + y\sin\phi) - p$$

is very small (usually a few nm) compared to the wavelength, so that an expansion of the exponential factor is allowed in Eq. (1):

$$\Gamma(R,\theta,\phi) = \int_{R^2} I_{w_1}(x,y)\,[1 + 2ik\,\delta f(x,y) - 2k^2 f(x,y)^2]\,dx\,dy.$$

The square modulus is then

$$|\Gamma(R,\theta,\phi)|^2 = 1 - 4k^2[\langle \delta f^2\rangle_{w_1} - \langle \delta f\rangle_{w_1}^2]$$

where we denote by $\langle F\rangle_w$ the weighted average of any function $F(x,y)$:

$$\langle F\rangle_w = \int_{R^2} I_w(x,y) F(x,y).$$

It is always possible to choose the dummy piston in such a way that $\langle \delta f\rangle = 0$, and we get

$$|\Gamma(R,\theta,\phi)|^2 = 1 - 4k^2\langle \delta f^2\rangle.$$

The maximum of $|\Gamma|^2$ is obviously attained when $\langle \delta f^2\rangle$ is a minimum, and eventually, the problem is thus strictly equivalent to fit a quadric polynomial

$$\hat{f}(x,y) = \frac{x^2+y^2}{2R} + \theta(x\cos\phi + y\sin\phi) + p$$

to the empirical function $f(x,y)$ by an intensity-weighted least-square algorithm. This is the way we proceed. This gives a better estimate of $1/2R$, $\theta\cos\phi$ and $\theta\sin\phi$, and the new value R_2 found for R gives in turn a better estimate of w. The procedure is iterated until a stable value is found for all parameters. At the end, the final function δf is the residual roughness, and $\langle \delta f^2\rangle$ is the weighted rms roughness. The tilt and the piston are removed by using $f'(x,y) = f(x,y) - \theta(x\cos\phi + y\sin\phi) - p$ instead of $f(x,y)$. f' represents a rough but collimated paraboloid (for the relevant beam), of which the curvature radius is accurately known. For instance, see Table I for two mirrors recently produced for the ends of the two arms of Virgo, coated at SMA-Lyon, referred to as C01077 and C02017, respectively.

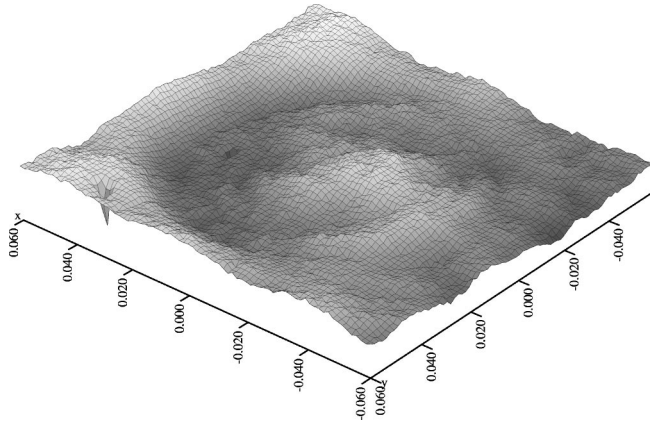

FIG. 1. Residual roughness in the central zone of C01077; (x,y) units are m. Weighted rms roughness: 2.8 nm.

Figures 1 and 2 show the structure of the residual roughnesses of the two mirrors, respectively. One can notice the analogy of the two profiles, up to a possible rotation.

B. Models of paraxial optical devices

We briefly describe the principles of the codes used for simulating operation of complex optical systems like gravitational wave interferometric detectors. In these devices, the light beams have very long (km) Rayleigh parameters and the mirrors are nearly flat (several km curvature radius), so that the paraxial approximation holds for describing light propagation. Two possible (called spectral) methods are valid in this context. They both consist of expanding the fields in elementary waves of which propagation is so simple that it results only in a phase factor. In the first one (Fourier transform technique), the field is expanded on a continuous family of plane waves. In the second (called modal), the field is expanded on a discrete family of Hermite-Gauss wave functions. Both families are orthogonal solutions of the paraxial (Fresnel) wave equation. We have developed the two approaches separately, firstly because their excellence area does

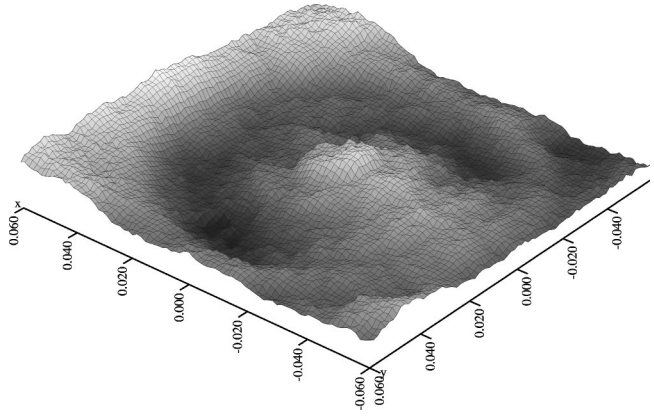

FIG. 2. Residual roughness in the central zone of C02077; (x,y) units are m. Weighted rms roughness: 3.6 nm.

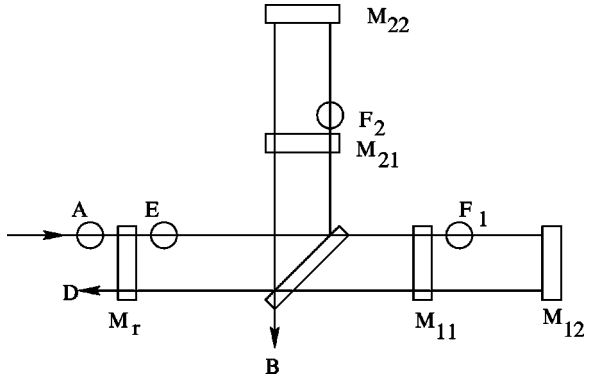

FIG. 3. Power recycling Michelson interferometer with Fabry-Perót cavities.

not exactly coincide and, secondly, in order to be able to check results by comparing the outputs of independent codes.

1. FFT based codes

The principle of light propagation by Fourier transforms, and its implementation via fast Fourier transform (FFT) has been described in [6]. Let us recall briefly that for the complex amplitude of any field being $A_0(x,y)$ at $z=0$, one can compute its new amplitude at a distance L by taking its 2D Fourier transform $\tilde{A}_0(p,q)$ and then multiplying it by the propagator (Fourier transform of the diffraction kernel),

$$P_L(p,q)=\mathrm{e}^{ikL}\,\mathrm{e}^{-i\lambda L(p^2+q^2)/4\pi}.$$

One finds the Fourier transform $\tilde{A}_L(p,q)=P_L(p,q)\times\tilde{A}_0(p,q)$ of the amplitude after propagation. The inverse 2D Fourier transform gives the amplitude $A_L(x,y)$ itself. The whole algorithm can be represented symbolically by the linear propagation operator $\mathcal{P}_L$ as

$$A_L=\mathcal{P}_L A_0\,.$$

The greatest interest of this technique is to reduce in practice the calculations to FFT calls. For this, we sample the amplitudes on a square grid, giving $N\times N$ arrays that enter the 2DFFT routines. Reflection on a mirror is represented by a product with a mirror operator $M(x,y)$. If $f(x,y)$ denotes the apex equation of the mirror's surface, and r its scalar photometric reflectivity (we assume it uniform), we have

$$M(x,y)=r\,\mathrm{e}^{2ikf(x,y)}$$

and if we denote by $A_0(x,y)$ the incoming amplitude and by $A_{\mathrm{ref}}(x,y)$ the reflected one, we have

$$A_{\mathrm{ref}}(x,y)=M(x,y)\times A_0(x,y)$$

so that whatever the simulated system, the code reduces in FFT's and simple array products in the direct and in the Fourier space. This allows us to benefit from any parallelization capability of the used workstation. Finding the fields inside a resonant cavity, and especially in a recycling interferometer requires [7] an iterative algorithm. For a power recycling system such as Virgo, we proceed as follows (see Fig. 3): We denote by R_i, T_i, respectively, the operators associated with the reflection and the transmission of mirror M_i. The 6 mirrors involved are the recycling mirror M_R, the corner mirror M_{11} and the far mirror M_{12} of the north cavity, and the corresponding M_{21}, M_{22} for the west cavity. The splitter is M_S. We start from three estimates (E,F_1,F_2) of the internal fields corresponding to the easily computed ideal situation (perfect mirrors), then new estimates can be computed according to the following scheme:

$$E^{\mathrm{new}}=T_R A+R_R[\mathcal{P}_1 R_{11}\mathcal{P}_1+\mathcal{P}_2 R_{21}\mathcal{P}_2]E^{\mathrm{old}}+R_R\mathcal{P}_1 T_{11}\mathcal{C}_1 F_1^{\mathrm{old}}+R_R\mathcal{P}_2 T_{21}\mathcal{C}_2 F_2^{\mathrm{old}}$$

$$F_1^{\mathrm{new}}=T_{11}\mathcal{P}_1 E^{\mathrm{old}}+R_{11}\mathcal{C}_1 F_1^{\mathrm{old}}$$

$$F_2^{\mathrm{new}}=T_{21}\mathcal{P}_2 E^{\mathrm{old}}+R_{21}\mathcal{C}_2 F_2^{\mathrm{old}}$$

where $\mathcal{C}_i$ denotes a round trip in cavity $\#i$ (i.e. propagation/reflection/propagation), $\mathcal{P}_1$ a propagation along the north short arm through the splitter, and $\mathcal{P}_2$ a propagation from south to west by reflection on the splitter. Then the process is iterated until the Hermitian distance between two successive estimates is small enough. At the end, the field in the dark fringe is B given by

$$B=[\mathcal{P}_1' R_{11}\mathcal{P}_1+\mathcal{P}_2' R_{21}\mathcal{P}_2]E+\mathcal{P}_1' T_{11}\mathcal{C}_1 F_1+\mathcal{P}_2' T_{21}\mathcal{C}_2 F_2$$

where the operators $\mathcal{P}_1'$ and $\mathcal{P}_2'$ represent, respectively, a propagation from north to east by reflection on the splitter, and a propagation from west to east through the splitter.

2. Modal codes

We denote by $\mathcal{H}_0$ the Hilbert space of optical amplitudes at $z=0$, and by $\mathcal{H}_L$ the Hilbert space of optical amplitudes at $z=L$. If we take in $\mathcal{H}_0$ a basis of Hermite-Gauss functions, $\{\varphi_{m,n;0}(x,y) : m,n\in\mathbf{N}\}$, and in $\mathcal{H}_L$ the basis $\{\varphi_{m,n;L}(x,y) : m,n\in\mathbf{N}\}$ involving the same TEM modes but diffracted over the distance L, propagation along a distance L of any optical field is a mapping $\mathcal{H}_0\to\mathcal{H}_L$, represented by the diagonal operator $\mathcal{P}$, acting as

$$\mathcal{P}\varphi_{m,n,0}=\mathrm{e}^{-i(m+n+1)\alpha}\varphi_{m,n,L}$$

where α is a constant depending on L and on the Rayleigh parameter b of the beam [namely $\alpha=\tan^{-1}(L/b)$]. The effect of mirrors on amplitudes can be represented by matrices

$$M_{mm'nn'}=\langle\varphi_{m',n',z}, M\varphi_{m,n,z}\rangle$$

where $\langle\ldots\rangle$ denotes the Hermitian scalar product. In practice, the infinite family of modes taken into account in a code must be truncated. It is consistent to take $m+n\leqslant V$, the total number of modes being then $N_M=(V+1)(V+2)/2$. With such a representation of propagation and reflection, all codes reduce to $N_M\times N_M$ matrix algebra.

3. A brief comparison

Both the discrete Fourier transform (DFT) approach and the modal expansion (ME) approach have in common a practical limit in their dimension. If $N\times N$ is the dimension of the arrays representing the fields in DFT's and V the maximum order of modes in ME's, we have the following numbers: $N_F=N^2$ for DFT, and $N_M=(V+1)(V+2)/2$ modes for ME. The information lost by this unwanted but necessary truncation has some similar consequences in the two approaches. Reducing N_F or N_M removes information on sharp details in the field. It forbids us to represent too large diffraction angles. But the main difference lies in the fact that a modal expansion matches more efficiently the nearly Gaussian mode of a realistic Fabry-Perót cavity than an expansion in terms of plane waves. As long as we are interested by small deviations with respect to the fundamental TEM_{00} of the cavity caused by smooth aberrations, ME-based codes can give excellent results with a N_M much smaller than the N_F which is necessary for reaching the same accuracy. If we are now interested in light scattered by the roughness of mirrors, the random details of the field are more easily matched by plane waves of any direction than with combinations of even higher order Hermite-Gauss modes of fixed waist, and DFT methods are preferable.

IV. MODE-CLEANER MIRRORS

The mode cleaner is a long ($\sim$143 m) triangular cavity designed to filter out jitter in the pointing of the laser beam and power fluctuations. It has the topology of a ring cavity in order to avoid spurious collimated reflections that could spoil the laser stability. This property results from the existence of a unique clockwise propagating mode. The two nearly orthogonal mirrors forming the basis are flat, whereas the far mirror is spherical. A special situation in the interferometer is that this mirror works under a small incidence angle. Due to its residual roughness, it is able to scatter light in a solid angle large enough to include the incoming direction, and thus to couple some power into the counterpropagating mode. This results in interference fringes on the detector that are able to make unstable the servo loops that are locking the cavity. As we shall see, the situation can be evaluated without any propagation algorithm. The coordinates are such that the z axis is the spherical mirror axis. The x,y axes are orthogonal and within the plane tangent to the mirror. We denote by $\varphi_0(x,y)$ an incoming Gaussian beam, matched to the mirror, and incident with angles (θ,ϕ). We have

$$\varphi_0(x,y)=\sqrt{\frac{2}{\pi w^2}}\exp[-(x^2+y^2)/w^2]\times\exp[-ik(x^2+y^2)/2R]\times\exp[-ik\theta(x\cos\phi+y\sin\phi)].$$

The mirror operator is

$$M(x,y)=\exp[2ikf(x,y)]$$

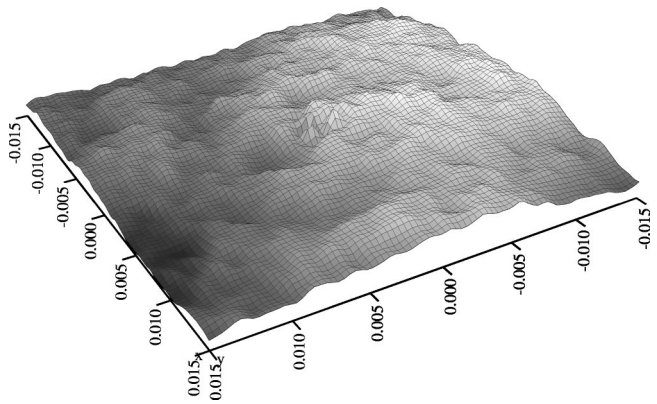

FIG. 4. Residual roughness in the central zone of the MC spherical mirror; (x,y) units are m. Weighted rms roughness: 2.8 nm.

where $f(x,y)$ refers to the wave front map of the mirror, including the mean paraboloid plus the residual roughness. The reflected beam is thus

$$\varphi_R(x,y)=M(x,y)\times\varphi_0(x,y).$$

The counterpropagating beam φ_c is the phase conjugate of φ_0,

$$\varphi_c=\overline{\varphi_0}.$$

The coupling coefficient $\Gamma(\theta,\phi)$ between the reflected and the counterpropagating beams is given by the Hermitian scalar product:

$$\Gamma(\theta,\phi)=\langle\varphi_c,\varphi_R\rangle$$

or, in detail,

$$\Gamma(\theta,\phi)=\int_{\mathbf{R}^2}I(x,y)\exp\left[2ik\left(f(x,y)-\frac{x^2+y^2}{2R}\right)\right]\times\exp[-2ik\theta(x\cos\phi+y\sin\phi)]dxdy$$

where $I(x,y)$ is the normalized intensity distribution in the beam. Note that the function $\delta f(x,y)\equiv f(x,y)-[(x^2+y^2)/2R]$ is nothing but the residual roughness of the mirror (see Fig. 4).

Since this residue is small compared to a wavelength, we can write

$$\Gamma(\theta,\phi)=\exp\left[-\frac{2\pi^2w^2\theta^2}{\lambda^2}\right]+2ik\int_{\mathbf{R}^2}I(x,y)\,\delta f(x,y)\times\exp[-2ik\theta(x\cos\phi+y\sin\phi)]dxdy-2k^2\int_{\mathbf{R}^2}I(x,y)\;\;\delta f(x,y)^2\times\exp[-2ik\theta(x\cos\phi+y\sin\phi)]dxdy.$$

When the roughness is zero, the first term still remains. It represents the natural overlap of the reflected beam with the phase conjugate beam, due to Gaussian divergence. If θ

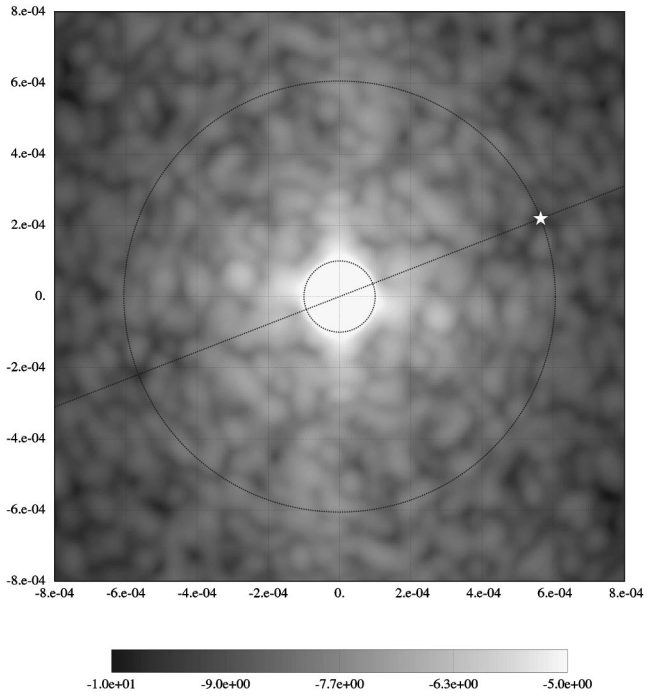

FIG. 5. Coupling coefficient as a function of (θ,ϕ) (logarithmic scale). The star shows the optimal orientation of the mirror.

$=0$, this overlap is simply unity, expressing the perfect matching of the beam. We can express the natural overlap as

$$\Gamma_0(\theta) = \exp[-2\theta^2/\theta_g^2]$$

where $\theta_g \equiv \lambda/\pi w$. For the Virgo mode-cleaner parameters, we have $\theta_g \sim 3.15\times10^{-5}$ Rd. For values of θ comparable to the mode-cleaner sharp angle ($\theta_{\rm MC}\sim 3\times10^{-4}$ Rd), we see that $|\Gamma_0|^2$ is extremely small and definitely negligible. Within the angular region corresponding to backscattering, it is thus possible to reduce the expression of the coupling factor to the accurate approximation

$$|\Gamma(\theta,\phi)|^2 = 4k^2 \left| \int_{\mathbf{R}^2} I(x,y)\ \ \delta f(x,y) \times \exp[-2ik\theta(x\cos\phi + y\sin\phi)]dxdy + ik\int_{\mathbf{R}^2} I(x,y)\ \ \delta f(x,y)^2 \times \exp[-2ik\theta(x\ \cos\ \phi + y\ \sin\ \phi)]dxdy \right|^2$$

showing that the result reduces eventually to the Fourier transform of the roughness, weighted, as usual, by the intensity distribution of the beam. For numerical computation, it is straightforward to use the exact formula

$$|\Gamma(\theta,\phi)|^2 = |\tilde{J}(2k\theta\cos\phi, 2k\theta\sin\phi)|^2$$

where $J(x,y) \equiv I(x,y)\ \exp[2ik\delta f(x,y)]$. We give in Fig. 5 a map of the backcoupling in angular coordinates. The outer thin circle corresponds to coupling with the counterpropagating beam for all azimuth angles of the incident beam, or as well for all rotations of the mirror around its axis. The inner thin circle surrounds a nonsignificant region where the natural overlap dominates, and which has been removed. We see that backcoupling depends sharply on this azimuth angle ϕ. One could raise the question of the sensitivity of this pattern with respect to the centering of the analyzing beam: in other words, has this pattern any physical reality? The answer can be obtained by varying via a small offset the incidence location on the mirror, then taking the average value of $|\Gamma|^2$ over all locations; we call this operation dithering. If we consider a Gaussian distribution of parameter δw of these incidence locations, dithering is strictly equivalent to taking an analyzing beam of width $w' = \sqrt{w^2 + \delta w^2}$. For plausible values of δw (analogous to an error in the centering), the map is rather unsensitive to small variations of w. We conclude that it has an actual physical meaning. It also shows that there are preferred orientations, and that these preferred orientations require a rather accurate positioning. Figure 6 represents the variations of $|\Gamma|^2$ along the outer circle, i.e. for all possible orientations of the mirror, the incidence angle being fixed. A hole in the speckle pattern is exactly on the circle at $\phi \sim 0.37$ Rd, and it gives a better position of the mirror.

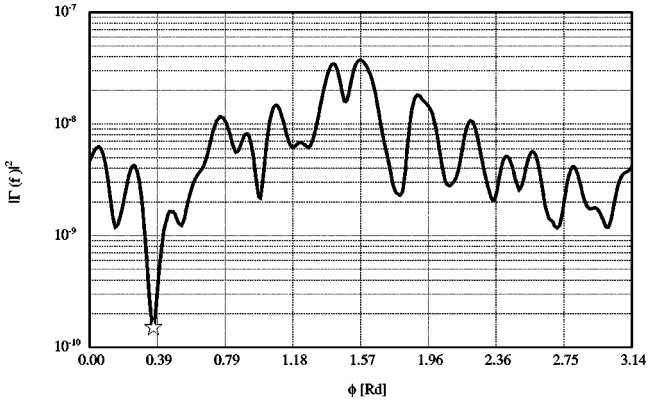

FIG. 6. Coupling coefficient as a function of ϕ for backscattering. The star locates the preferred orientation as pointed out in the preceding map.

V. VIRGO END MIRRORS

A. Orientation

We now consider a recycling interferometer involving the two mirrors of which the main parameters have been extracted, namely C01077 and C02017. We can define a merit factor for the interferometer by an expression analogous to the signal to noise ratio. It is well known that the SNR is (i) proportional to the square root of the recycled power and (ii) proportional to the finesse at low frequency. P is the power operator acting on amplitudes, the recycled power can be estimated from $P(E)$, and the finesses of the cavities from the ratio $P(F_i)/P(E)$. We have performed the computation of the SNR for various relative orientations of the mirrors and got the following results (see Fig. 7) It seems clear that the two mirrors should be given the same orientation. This could be surprising, and even could raise suspicion against

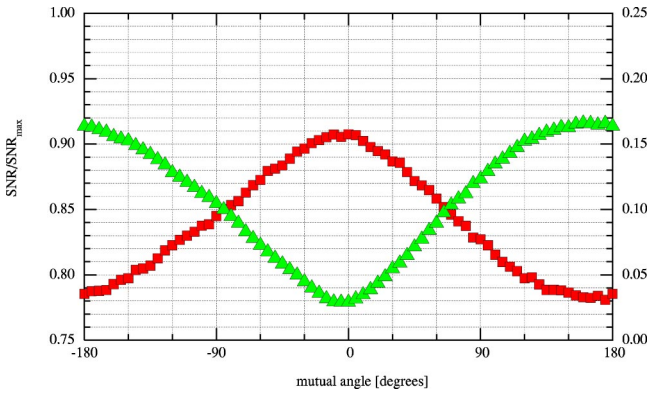

FIG. 7. SNR vs a mutual angle of end mirrors (squares). SNR_{max} corresponds to identical and perfect mirrors. Integrated power on dark fringe (triangles).

the correctness of the codes, if we did not know that the mirror substrates are manufactured with two parallel flats on the edge (in order to allow further bonding processes), before polishing. The flats obviously suppress any arbitrariness in the positioning of the blanks in the polishing device. The two blanks have thus undergone almost identical actions (examine the roughness patterns of Figs. 1 and 2) in identical positions; this explains why they must eventually also work in the same position. In the case where the mirrors are optimally installed, they have nevertheless different curvature radii, and consequently the waist of the two TEM_{00} cavity modes are different. One could ask what is the best beam parameter for the laser source. The answer can be drawn from Fig. 8: We see that the actual value of the input waist is noncritical. We see also that the losses in the SNR come not from the curvature differences, but from the roughness. The best dark fringe (obtained with the optimal position of the mirrors) has the structure showed on Fig. 9.

B. Scattered light

The numerical map allows us to also get some information about the scattered light distribution. This information is limited by the maximum diffraction angle allowed by the

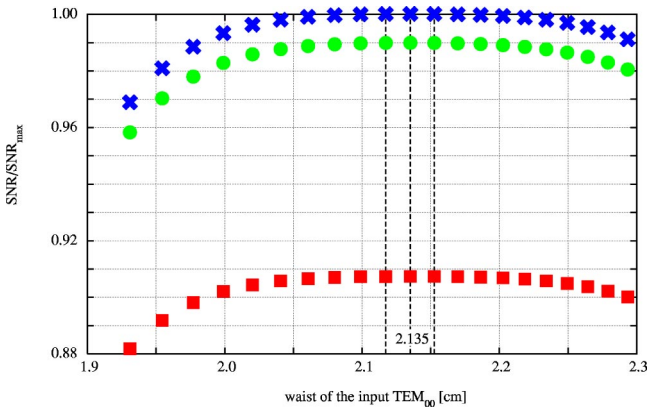

FIG. 8. SNR versus waist of the input TEM amplitude. Crosses: two identical mirrors with zero roughness. Circles: different curvatures and no roughness. Squares: actual situation.

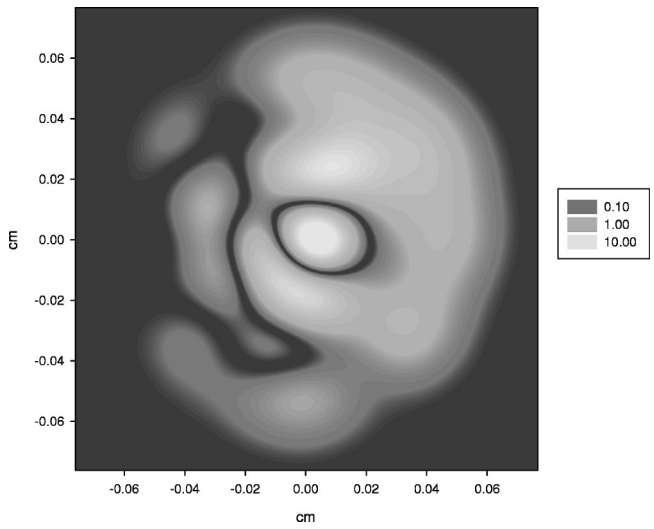

FIG. 9. Intensity distribution in the optimal dark fringe structure (logarithmic scale).

DFT principles. For a computational window of width a, the quantum of frequency in the Fourier space is $\delta p = 2\pi/a$, and consequently the frequency dynamics is $p_{max} = N\pi/a$ if N is the common number of samples along the x and y directions. If we interpret the spatial frequencies (p,q) (coordinates in the Fourier space) as projections on the transverse plane of oblique wave vectors, according to

$$p = (2\pi/\lambda)\,\theta\cos\phi, \quad q = (2\pi/\lambda)\,\theta\sin\phi, \tag{2}$$

we have an estimate of the maximum diffraction angle allowed:

$$\theta_{max} = \frac{N\lambda}{2a}.$$

For a 1 m wide window with 256×256 samples, this means $\theta_{max} \sim 1.28\times10^{-4}$ Rd. This may seem very restrictive, but it allows us to explore an angular region very problematic for the experiment. Larger values are difficult to test numerically (to get one order of magnitude, the size the grid should increase by 2 orders of magnitude) but can be experimentally explored, so that there is a natural complement between direct measurements and numerical treatment. Let us assume that a perfectly Gaussian beam $(TEM_{00})\,\phi_{00}(x,y)$ is reflected by a mirror of apex equation $z = (x^2+y^2)/2R + \delta f(x,y)$, where R is the curvature radius of the mirror, and $\delta f(x,y)$ its residual roughness. The Fourier transform of the reflected beam $\Psi(x,y)$ is

$$\tilde{\Psi}(p,q) = \int_{\mathbf{R}^2} e^{i(px+qy)} e^{ik(x^2+y^2)/R + 2ik\delta f(x,y)} \times \phi_{00}(x,y)\,dx\,dy. \tag{3}$$

If the peak-to-peak amplitude of the roughness is much less than the wavelength (otherwise the mirror is useless), we can expand $\exp 2ik\delta f$, which yields

$$\tilde{\Psi}(p,q)=\widetilde{\phi'_{00}}(p,q) + 2ik\int_{\mathbf{R}^2} e^{i(px+qy)}\,\delta f(x,y)\,\phi'_{00}(x,y)\,dx\,dy$$

where we denote by ϕ'_{00} the amplitude that would be reflected in the absence of roughness, i.e. the phase conjugate of the incoming TEM_{00}. We call this part specularly reflected. We are interested in the difference between the specular and the non-specular parts in the actual reflection, and more specifically in

$$|\tilde{\Psi}(p,q)-\widetilde{\phi'_{00}}(p,q)|^2 = 4k^2\int_{\mathbf{R}^2} e^{i[p(x-x')+q(y-y')]}\phi'_{00}(x,y)\,\overline{\phi'_{00}(x',y')} \times \delta f(x,y)\,\delta f(x',y')dx\,dy\,dx'\,dy'. \quad (4)$$

If we consider the (virtual) class of all mirrors that have been manufactured exactly the same way, we can view $\delta f(x,y)$ as a random process, characterized by two statistical moments, namely a zero mean and a rms value

$$\langle \delta f^2\rangle=\sigma^2.$$

The random process δf, considered stationary on the mirror surface, has an autocorrelation function $C(x,y)$ such that

$$\langle \delta f(x,y)\ \ \delta f(x',y')\rangle = \sigma^2 C(x-x',y-y') = \frac{\sigma^2}{4\pi^2}\int_{\mathbf{R}^2} e^{-i[p'(x-x')+q'(y-y')]}\tilde{C}(p',q')dp'dq'. \quad (5)$$

We get, after some elementary algebra

$$\langle|\tilde{\Psi}(p,q)-\widetilde{\phi'_{00}}(p,q)|^2\rangle = \frac{k^2\sigma^2}{\pi^2}\int_{\mathbf{R}^2}\tilde{C}(p',q')|\widetilde{\phi'}_{00}(p-p',q-q')|^2dp'dq' = 4k^2\sigma^2\tilde{D}(p,q). \quad (6)$$

The quantity $\tilde{C}(p,q)$ appearing in the preceding formulas is the power spectral density of the process *f*. It represents the distribution of the various spatial frequencies in the scattered light. It is likely that this distribution is much wider than the angular extension of the specularly reflected light. This can be seen by considering the inverse Fourier transform of $\tilde{D}$ which is simply the product of the Gaussian intensity by the autocorrelation function:

$$D(x,y)=C(x,y)\times I(x,y).$$

The autocorrelation function $C(x,y)$ is sharply peaked with a correlation range much shorter than the beam width *w*, so that the Gaussian intensity is practically constant through the significant part of the autocorrelation function. This does not exclude some long range correlation due to large scale aberrations, but if this happens, it is in a region where $I(x,y)$ is negligible. It is equivalent to replacing in Eq. (6), $|\widetilde{\phi'}_{00}(p,q)|^2$ by a delta function, and finally

$$\langle|\tilde{\Psi}(p,q)-\widetilde{\phi'_{00}}(p,q)|^2\rangle=4k^2\sigma^2\tilde{C}(p,q). \quad (7)$$

Now, the power spectral density can be interpreted as an angular density of scattered light according to (see [4])

$$\tilde{C}(k\theta\cos\phi,k\theta\sin\phi)=\frac{\lambda^2}{4k^2\sigma^2}\frac{dP_{\text{scatt}}(\theta,\phi)}{P_{\text{in}}\ d\Omega}.$$

In order to get a simple merit function for a given mirror, we take an azimuthal average over ϕ:

$$\frac{dP_{\text{scatt}}(\theta)}{P_{\text{in}}\,d\Omega}=\frac{1}{\lambda^2}\langle|\tilde{\Psi}(p,q)-\widetilde{\phi'_{00}}(p,q)|^2\rangle=P(\theta) \quad (8)$$

where (p,q) are implicitly assumed, expressed as functions of (θ,ϕ).

The numerical computation is easy to perform on the numerical maps by processing the mirror for various rotation angles and taking the average distribution. We then get the plots of $P(\theta)$ for the two mirrors (Fig. 10). The function $P(\theta)$ is analogous to the bidirectional reflection distribution function (BRDF) of the mirror (frequently used for surface characterization) for normal incidence. This averaged distribution allows us to easily compare different mirrors. Here, the similarity of the two distributions is clear, and is one more proof of the homogeneity of the manufacturing process from its beginning. The line θ_g corresponds to the angle at which the specular beam intensity is $1/e^2$ times its maximum value. The line θ_M corresponds to the edge of the facing flat mirror seen from the end mirror, in other words, light with a scattering angle larger than θ_M escapes the cavity.

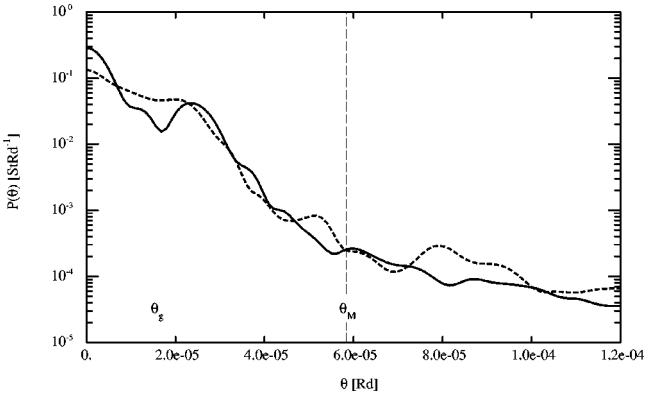

FIG. 10. Relative angular distribution of scattered light. Solid line: C01077; dashed line: C02017. θ_g: Gaussian divergence of the specularly reflected beam; θ_M: edge of the facing mirror.

VI. CONCLUSION

Some useful information can be extracted from the wave front maps measured on mirrors recently produced for Virgo.

We have shown how to compute the best orientation of the mirrors either for minimizing the backscattering or for maximizing the signal to noise ratio of the interferometer. We also show how to obtain the part of the scattered light angular distribution near the axis but outside the facing mirror, in an angular region where direct measurements are difficult.

[1] Public documents about the Virgo project can be found at http://www.virgo.infn.it
[2] Public documents about the LIGO project can be found at http://www.ligo.caltech.edu
[3] M. Barsuglia, F. Bondu, H. Heitmann, Ph. Heusse, C.N. Man, and L. Matone, Rev. Sci. Instrum. **71**, 1 (2000).
[4] J-Y. Vinet, V. Brisson, and S. Braccini, Phys. Rev. D **54**, 1276 (1996).
[5] J-Y. Vinet, V. Brisson, S. Braccini, I. Ferrante, L. Pinard, F. Bondu, and E. Tournié, Phys. Rev. D **56**, 6085 (1997).
[6] P. Hello, C.N. Man, A. Brillet, and J-Y. Vinet, J. Phys. I **2**, 1287 (1992).
[7] L. Pinard, P. Ganau, J-M. Mackowski, C. Michel, M. Napolitano, and E. Vireton, Tech. Dig. Ser.-Opt. Soc. Am. **17**, 200 (1995).
[8] Daniel Malacara, *Optical Shop Testing* (John Wiley & Sons, New York, 1992), Chap. 1.